Two localized CO_2 laser treatment methods for mitigation of UV damage growth in fused silica*

Jiang Yong(蒋 勇)[a)b)], Xiang Xia(向 霞)[a)†], Liu Chun-Ming(刘春明)[a)], Luo Cheng-Si(罗成思)[a)], Wang Hai-Jun(王海军)[b)], Yuan Xiao-Dong(袁晓东)[b)], He Shao-Bo(贺少勃)[b)], Ren Wei(任 玮)[b)], Lü Hai-Bing(吕海兵)[b)], Zheng Wan-Guo(郑万国)[b)], and Zu Xiao-Tao(祖小涛)[a)‡]

[a)] *Department of Applied Physics, University of Electronic Science and Technology of China, Chengdu* 610054, *China*
[b)] *Research Center of Laser Fusion, China Academy of Engineering Physics, Mianyang* 621900, *China*

(Received 23 August 2011; revised manuscript received 27 September 2011)

Two methods: high-power, short-time, single-shot irradiation (Method A) and low-power, long-time, multi-shot irradiation (Method B) are investigated to mitigate the UV damage growth in fused silica by using a 10.6-μm CO_2 laser. To verify the mitigation effect of the two methods, the laser induced damage thresholds (LIDTs) of the mitigated sites are tested with a 355-nm, 6.4-ns Nd:YAG laser, and the light modulation of the mitigation sites are tested with a 351-nm continuous Nd:YLF laser. The mitigated damaged sites treated with the two methods have almost the same LIDTs, which can recover to the level of pristine material. Compared with Method A, Method B produces mitigated sites with low crater depth and weak light modulation. In addition, there is no raised rim or re-deposited debris formed around the crater edge for Method B. Theoretical calculation is utilized to evaluate the central temperature of the CO_2 laser beam irradiated zone and the radius of the crater. It is indicated that the calculated results are consistent with the experimental results.

Keywords: fused silica, CO_2 laser mitigation, light modulation, damage threshold

PACS: 42.70.Ce,78.20.–e, 78.20.Bh, 79.20.Eb **DOI:** 10.1088/1674-1056/21/6/064219

1. Introduction

In the high-power laser systems, the optical components are subjected to high fluence 3ω laser irradiation. Fused silica is the most developed substrate material used in the systems for large aperture components. At present, there appear few defects and little surface damage in the large aperture optics after being treated by the advanced grinding and polishing techniques such as magnetorheological finishing[1,2] and off-line laser conditioning before putting them into practical applications.[3,4] The laser induced damage threshold (LIDT) of the large aperture optics is also enhanced accordingly after conditioning it by these technologies. However, some defects still remain in the surface and/or sub-surface of fused silica. Once the defects are damaged under high fluence 3ω laser illumination, the damage will grow exponentially under subsequent laser shots, and it may lead to a catastrophic damage, which is a major concern for the durability of the optical components.[5]

In order to arrest the damage growth and extend the life-time of the optical components, a feasible mitigation process is necessary. Various protocols including chemical treatment,[6,7] plasma etching,[8,9] micro-flame torch processing,[8,9] and CO_2 laser treatment[10−13] are used for mitigation. CO_2 laser treatment is the most promising method to mitigate the damage growth of fused silica in those protocols.[14,15] It is used not only to polish the fused silica surface to increase the laser damage resistance by eliminating the small defects (scratches, pits, etc.) and contaminant on the surface of fused silica,[16] but also to mitigate the initial damaged sites of various sizes by high temperature melting.[14,15] However, some raised rims or re-deposited debris are observed around the mitigation sites conditioned with

*Project supported by the Joint Fund of the National Natural Science Foundation of China and the China Academy of Engineering Physics (Grant No. 11076008), the Fundamental Research Funds for the Central Universities (Grant No. ZYGX2011J043), the Foundation for Young Scholars of University of Electronic Science and Technology of China (Grant No. 8010401JX0806), and the Young Scientists Foundation of Sichuan Province of China (Grant No. 2010JQ0006).

†Corresponding author. E-mail: xiaxiang@uestc.edu.cn
‡Corresponding author. E-mail: xtzu@uestc.edu.cn

© 2012 Chinese Physical Society and IOP Publishing Ltd

CO_2 laser, which will result in strong light modulation or damage re-initiation. Thus further investigation is very important to obtain mitigated sites free from raised rim or re-deposited debris.

In this work, the damaged sites with lateral dimension (L) < 400 μm and depth < 100 μm are mitigated with a 10.6-μm CO_2 laser by two different methods: high-power, short-time, single-shot irradiation (Method A) and low-power, long-time, multi-shot (Method B) irradiation. The remainder of the present paper is organized as follows. In Section 2, the experimental setups and mitigation parameters are presented. In Section 3, the crater profile and the relationship between the number of bubbles and damaged size are presented. In Section 4, theoretical calculation is used to evaluate the central temperatures and radii of craters of the sites mitigated with the two methods. Meanwhile, the advantages and disadvantages of the two methods are compared. In Section 5, the modulation to the incident laser beam induced by mitigation sites is measured with a 351-nm laser. In Section 6, the LIDT of sites mitigated with the two methods are tested with a 355-nm laser. Finally, the optimal method is obtained through the experimental results and theoretical analysis for the two mitigation methods.

2. Experimental details

Polished fused silica (Corning HPFS 7980) samples of nominal size 40 mm×60 mm×5 mm are etched in the buffered hydrofluoric (HF) acid solutions (1 wt% HF + 15 wt% NH_4F, pH=5) for 10 min to remove the deposited polishing material and reveal the defects before the experiment. A mono-longitudinal mode Nd:YAG pulse laser operated at 355 nm with a pulse width of 6.4 ns is used to create damaged sites with values of lateral size L ranging from 50 μm to 400 μm, i.e., 50 μm < L <400 μm, and test the LIDTs of pristine material and mitigation sites. The beam has a Gaussian spatial profile and is focused to 0.5-mm beam diameter at the exit surface of the fused silica sample, which is characterized by a Spiricon beam analyzer. The damaged sites less than 50 μm in diameter are first initiated in the output surface of the sample by using a 355-nm laser at a higher fluence, and then subjected to the "growth" shots at a lower fluence till the expected damaged size is obtained.

A schematic diagram of the mitigation setup is shown in Fig. 1. A commercial 10.6-μm CO_2 laser (Coherent) is used to mitigate the damaged sites. The laser has a maximum average power of 100 W and a maximum frequency of 25 kHz. The laser operates with an approximately Gaussian spatial profile, and the exit beam is a large TEM_{00} (> 95%) spot with a diameter of about (3.8±0.4) mm at $1/e^2$-fold intensity. The laser beam used for mitigation is obtained with a 10-cm focal length ZnSe lens. The transmission rate is about 85%.

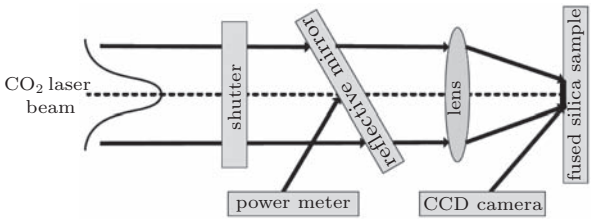


Fig. 1. Schematic diagram of the mitigation setup.

The damaged sites are mitigated by Methods A and B each with three sizes of CO_2 laser beams, 2 mm, 3 mm, and 7 mm in diameter. For Method A, the appropriate combination of laser power and irradiation time is selected to completely repair the damaged sites with single-shot irradiation. For Method B, the ramped powers are chosen to repair the damaged sites by multi-shot irradiation, i.e., the damaged sites are first preheated with a lower laser power, and then irradiated by increasing power until the crack structure is completely melted. No matter which method is selected, it is necessary to ensure that the damaged sites including the propagated cracks are completely healed by melt movement or removed by evaporation. In Table 1 are listed the mitigation parameters for different sizes of damaged sites used in this study. Considering the fluctuation of CO_2 laser power, the parameters are unchanged. However, the practical parameters may fluctuate during the mitigation process, which depends on the practical characterizations of the damaged sites, such as lateral size, depth, etc.

Table 1. CO_2 laser mitigation parameters for different sizes of damaged sites.

	2 mm for 50 μm < L < 150 μm	3 mm for 150 μm < L < 250 μm	7 mm for 250 μm < L < 400 μm
Method A	20.2 W, 4 s, 1 shot	34.2 W, 5 s, 1 shot	97 W, 4 s, 1 shot
Method B	8.2 W, 4 s, 2 shots	16.1 W, 4 s, 2 shots	48.7 W, 10 s, 2 shots
	9.5 W, 4 s, 2 shots	19.2 W, 4 s, 2 shots	50.0 W, 10 s, 2 shots
	12.9 W, 4 s, 2 shots	22.5 W, 4 s, 2 shots	56.6 W, 10 s, 2 shots

A commercial Nd:YLF multi-wavelength laser (Photonics) is used to measure the modulation to the incident laser beam induced by the mitigation sites. The sketch of the measurement setup is shown in Fig. 2. The laser is acousto-optically Q-switched and operated at 5 kHz, which can simultaneously emit three wavelengths: 1053 nm, 527 nm, and 351 nm. The wavelength used in this experiment is selected by a laser wavelength pass filter (WF). The laser is spatially filtered (SF) by a 20-μm pinhole and collimated by an uncoated 40-cm fused silica lens. A green cw-HeNe beam is used as a visible alignment source for the collimation beam. A digital CCD camera is mounted on a 40-cm translation stage to record the diffraction pattern at different distances. The modulation values are calculated for each diffraction image at the corresponding location.

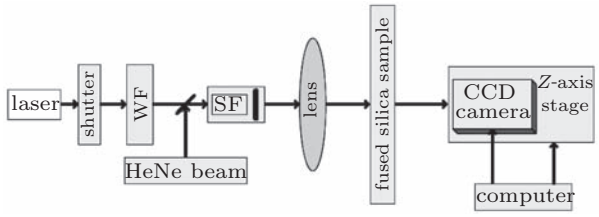


Fig. 2. Sketch of the light modulation measurement setup.

The morphologies of the damaged and mitigation sites are observed by a Nikon optical microscope. The profile trace of the mitigation site is measured by a stylus profilometer. After being mitigated, the samples are annealed in a clean furnace at 850 °C for 10 h to eliminate the residual stress induced by CO_2 laser irradiation in the ambient atmosphere. Then the annealed samples are etched for 15 min in a buffered HF acid solution (1 wt% HF + 15 wt% NH_4F, pH=5) to remove the re-deposited debris and possible contaminants on the fused silica surface. Finally, the LIDT test is performed for the mitigated sites.

3. Crater profile and bubbles

In order to depict the experimental results and compare the mitigation effects induced separately with small and large-spot laser beams, the results for 2-mm and 7-mm CO_2 laser beams are selected. Figures 3(a) and 3(b) show the microscopic images of the typical sites mitigated by Methods A and B with a 2-mm CO_2 laser beam, respectively. Comparing two images, the distorted zone shown in Fig. 3(a) is larger than that in Fig. 3(b). The stylus profilometric traces of the two sites are shown in Figs. 3(a1) and 3(b1), indicating that the depth of site mitigated with Method A (Fig. 3(a1)) is larger than that with Method B (Fig. 3(b1)). In addition, the re-deposited debris can be observed around the mitigation site in Fig. 3(a). The observation by optical microscope shows that the re-deposited debris is always formed around the mitigation sites during the Method A mitigation process. The microscopic images of the 7-mm CO_2 laser beam mitigated damaged sites are not given here because the laser distorted zone is larger than the view field of the optical microscope. Re-deposited debris can also be observed around the sites mitigated with Method A for the case of the 7-mm beam. Similar to the site mitigated with the 2-mm beam, the site mitigated with Method A has a larger depth (Fig. 4(a)) than with Method B (Fig. 4(b)) when the 7-mm beam is used. Dai *et al.*[17] reported on different crater profiles of the sites mitigated with single-shot irradiation (Method A). In contrast, the sites mitigated with Method B have similar crater profiles even when different mitigation parameters are applied.

Compared with Method A, Method B is easy to obtain a crater with lower depth and produce less re-deposited debris. However, a few small spherical bubbles are observed in the sites mitigated with Method B, both for the 2-mm and 7-mm CO_2 laser beams. In contrast, there are no bubbles observed in the sites mitigated with Method A. The number of bubbles increases with the dimension of the damaged site increasing as shown in Fig. 5. The result is consistent with the result mitigated with 4.6-μm CO_2 laser beam reported by Guss *et al.*[18] The number of bubbles increases dramatically when the damage size $L > 500$ μm, which may be related to the effective irradiation area of the CO_2 laser beam and the selected mitigation parameters. This will be discussed in Section 4.

Although Method B has some advantages, more attention must be paid to further improving the bubble formation. The selected parameters influence not only the number of the bubbles, but also the dimension of the laser affected zone. The heat accumulation effect may result in the melting of some material around the crater when the power becomes high enough as shown in Fig. 4(b). Although the depth and the radius of the crater mitigated with the 7-mm CO_2 laser beam shown in Fig. 4(a) are less than those shown in Fig. 4(b), the affected zone of sites mitigated with Method B will give a larger negative influence on wavefront quality of optical components than the sites mitigated with Method A. Thus further investigation is necessary in order to improve the crater profile mitigated with Method B.

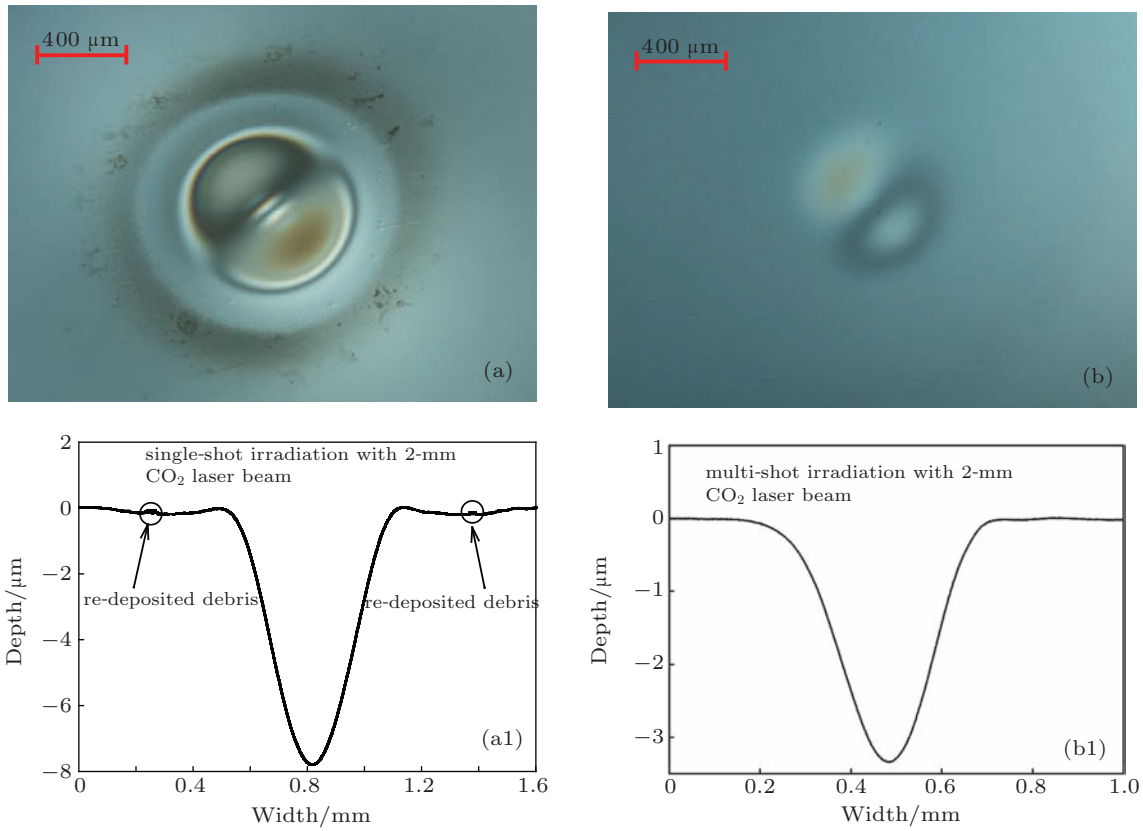


Fig. 3. (colour online) Microscopic images of typical site mitigated by the Methods A (a) and B (b) with 2-mm CO_2 laser beam, and the corresponding stylus profilometric traces of the sites ((a1) and (b1)).

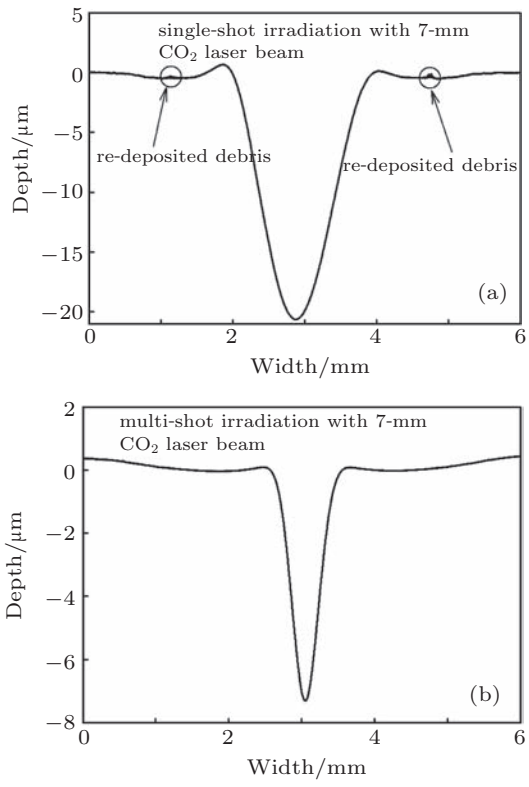


Fig. 4. Stylus profilometric traces of the craters mitigated with 7-mm CO_2 laser beam, with (a) Method A and (b) Method B.

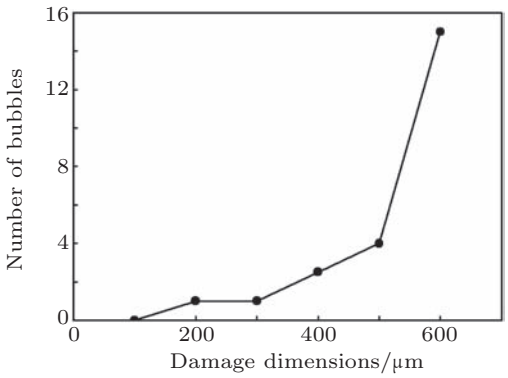


Fig. 5. Relationship between average number of bubbles and damage size.

4. Temperature evaluations during mitigation

As discussed above, different depths of craters can be obtained via different mitigation methods. Redeposited debris and raised rim are also observed around the sites mitigated with Method A. The morphologies and profiles of the craters are usually determined by the mitigation methods.

As is well known, the fused silica material has a

very high absorption coefficient and small absorption depth at 10.6 μm.[19,20] In order to melt the damaged material and cracks completely, it must be ensured that the temperature reaches the melting point at least. The melt and ablation velocity is directly related to the temperature in the damaged sites. For the Gaussian beam of radius r, the temperature in the centre of the laser spot is[21,22]

$$T_{\rm s} = \frac{AI\sqrt{\pi}}{2\kappa} r = \frac{AP}{2\sqrt{\pi}\kappa r}, \tag{1}$$

where A is the absorption coefficient, P is the laser power, κ is the thermal conduction coefficient, and I is the light intensity. It indicates that the steady state temperature decreases as laser beam size increases when the power is constant.

Taking the 7-mm CO_2 laser beam for example, the value of thermal conductivity is 0.02 W/cm·K at room temperature, for Methods A and B, the temperatures in the central laser beam, calculated with Eq. (1), are 3323 K and 1939 K, respectively, where 1939 K is calculated by the maximum power selected for Method B. For fused silica material, the melting point is 2300 K, and the ablation point is 3180 K.[10,23,24] In this case, the material removal rate of Method A is much larger than that of Method B because of the higher temperature, and the clear raised rim is observed around the edge of craters. For Method B, though the temperature does not reach the melting point for each shot, there is a thermal accumulation effect because of the ramped power mitigation process, so the damage and cracks can be completely healed.

However, the damaged site may not be preheated fully during the preheating at the lower power, which results in the generation of bubbles. In addition, mitigating a large damaged site with a smaller CO_2 laser beam may also lead to the generation of bubbles. The effective beam of the CO_2 laser cannot melt the whole damaged material. As the upper crack closes, the unhealed crack traps air and forms a bubble. Based on the two considerations mentioned above, a 2-mm CO_2 laser beam is chosen to mitigate the damaged sites with values of size L being smaller than 150 μm, i.e., $L < 150$ μm, in this study. A 3-mm CO_2 laser beam is chosen to mitigate the damaged sites sized in a range of 150 μm $< L <$ 250 μm. For the damaged sites with sizes ranging from 250 μm to 400 μm, a 7-mm beam is chosen. The fluctuation of practical power depends on the features of the damaged sites.

The steady state temperature distribution along the axis of the laser spot as a function of the depth (z) and the radius (R) of crater is given by[21]

$$T(z) = T_{\rm s}\, {\rm e}^{(z/r)^2} {\rm erfc}\left(\frac{z}{r}\right), \tag{2}$$

$$R = \sqrt{\frac{2T_{\rm s}K}{U}} r, \tag{3}$$

where U is the latent heat of evaporation per atom, and its value is 3.6 eV for fused silica; K is the Boltzmaman constant, $K = 1.38\times10^{-23}$ J/K. From Eq. (2), the depth of the melt is approximately equal to the beam size and the shape of the crater profile is independent of the thermal conductivity,[21] which is related only to the temperature at the centre of the CO_2 laser beam on the surface ($T_{\rm s}$) of fused silica. Substituting the temperature value given by Eq. (1) into Eq. (2) to evaluate the temperature at a certain depth, it is found that the depth of crater mitigated with Method A is larger than that with Method B. The phenomena are observed from experimental results measured by stylus profilometer shown in Figs. 3(a1), 3(b1), and Fig. 4, which are consistent with the theoretical analysis.

For the radius of the mitigated crater, taking the 7-mm CO_2 laser beam for example again, for Methods A and B, the radii of the craters calculated by Eq. (3) are 2.8 mm and 2.1 mm, respectively. The measured values shown in Fig. 4(a) is 2.2 mm (Method A), and 1.1 mm (Method B) in Fig. 4(b). The theoretical calculations are close to the experimental measurement, especially for Method A. The large difference for Method B probably results from the inaccurate evaluation of temperature because the heat accumulation by multi-shot irradiation is not taken into consideration and the temperature used for Eq. (3) is not a real value. In addition, thermal conductivity is assumed to be constant in this calculation. As is well known, the thermal conductivity increases with temperature increasing, which is the key parameter determined by the temperature rise.[22] Thus the calculation values are not very accurate since the thermal conductivity used for calculation is the value at 800 K.

5. Downstream intensification

The mitigated damaged sites can produce downstream intensification of the 351-nm light by ray focusing and a non-linear propagation process, which could potentially cause damage to another optical

component.[18,25] In this study, the diffraction patterns at a discrete distance downstream from each mitigated site are measured by the system in Fig. 2 and the modulation values are calculated for each diffraction pattern at the corresponding distance.

Several factors may influence the real value of modulation. The practical value of modulation (M) is calculated by the following equation:[26]

$$M = \frac{D}{F} = \frac{D_{\text{means}} - B}{F_{\text{means}} - B}, \tag{4}$$

where D_{means}, F_{means}, and B are the modulation of mitigation sites, empty field (the site is moved out of the view field), and ambient light background, respectively.

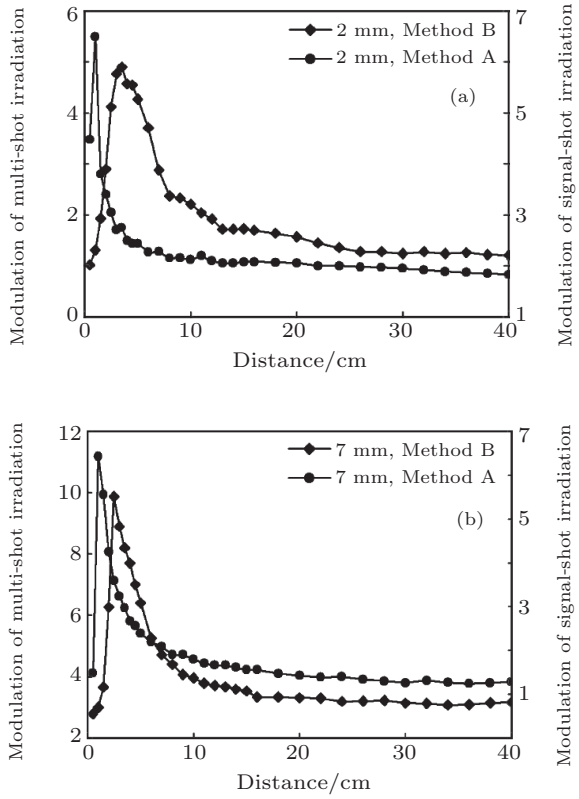


Fig. 6. Modulations of craters mitigated by the two methods with 2-mm and 7-mm CO_2 laser beams. The profiles of the measured sites are corresponding to Figs. 3(a1), 3(a2), and Fig. 4.

The results of mitigated sites corresponding to Figs. 3(a1), 3(b1), and Fig. 4 are shown in Fig. 6. It is found that the modulation of sites mitigated with Method A is larger than that with Method B, both for 2-mm and 7-mm CO_2 laser beams. This should be ascribed to the raised rim around the mitigated sites, because the raised rim surrounding a nominally circular mitigation site will produce an on-axis hot-spot that can be intense enough to damage downstream optical surfaces.[14,27] In addition, the height of the raised rim mitigated with the 7-mm CO_2 laser beam is larger than that with the 2-mm CO_2 laser beam (Fig. 4), which can contribute more to light modulation as shown in Fig. 6. In addition, the width and the depth of the mitigated site also contribute to the value of modulation. A comparison between the two mitigation methods indicates that a smooth round crater without a raised rim can effectively reduce the value of modulation. In addition, a crater with small width and depth can also reduce the modulation. Thus a smaller CO_2 laser beam and multi-shot irradiation are better for damage growth mitigation and the selected parameters should be optimized according to the requirement that the damaged sites are completely repaired without embedded bubbles.

6. Damage threshold and lifetime tests

Two damage test procedures are used to validate the mitigation effect of the two methods. One is the R-on-1 damage threshold test; the other is the damage lifetime test. Each test is performed on at least 15-mitigated sites. The re-deposited debris on sites mitigated with Method B have been completely eliminated by etching for 15 min in the buffered HF (1 wt% HF + 15 wt% NH_4F, pH=5) acid solution. It is shown that the average LIDT of pristine material is 9.05 J/cm^2. The average LIDTs of sites mitigated with Methods A and B are 8.98 J/cm^2 and 8.94 J/cm^2, respectively. The results of the life time test show that the pristine material and the entirely-mitigated sites for Methods A and B can survive withstand 200 shots at 7.03 J/cm^2, while about 80% of the tested sites of substrate and mitigation sites are damaged at 7.5 J/cm^2 during the life-time test. However, it should be pointed out that the average LIDT of sites mitigated by Method B is obtained from the sites free of bubbles. The average LIDT of mitigated sites tested by R-on-1 will decrease to 7.6 J/cm^2 if some bubbles appear. Figures 7(a) and 7(b) are the side-view images of the mitigation sites before and after the damage test, respectively, which indicate that the bubbles tend to damage by subsequent laser shots. Thus the formation of bubbles should be avoided during the mitigation process.

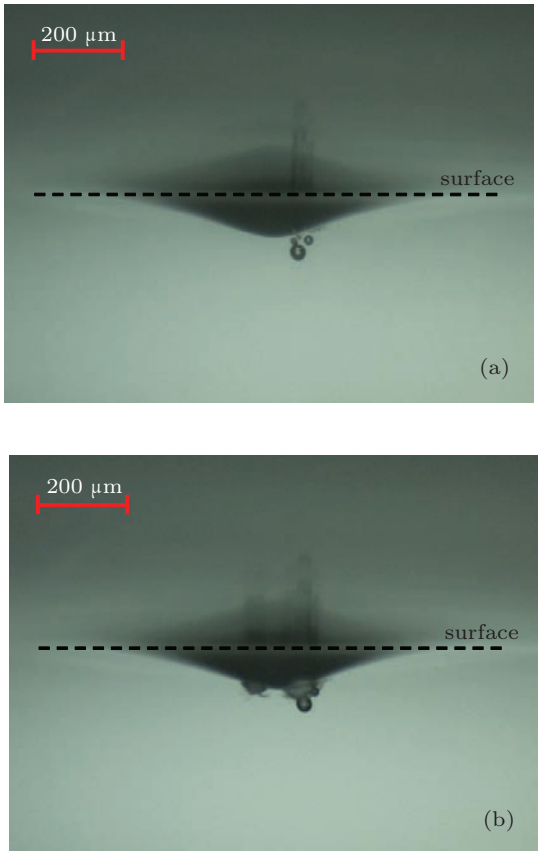


Fig. 7. (colour online) Side-view images of the bubbles before (a) and after (b) 355-nm laser irradiation.

From the viewpoints reported by Adams *et al.*[12] for a mitigation protocol to be acceptable, three basic acceptability requirements must be satisfied. Firstly, the protocol must prevent the re-initiation and/or growth of a damaged site by subsequent exposure to UV laser pulses. They pointed out that mitigated damaged sites can survive the testing at 3ω, 5 ns, up to larger than 12.5 J/cm^2 with $a < 3\%$ re-initiation rate.[12] The average LIDT of mitigated sites recover to the value of pristine fused silica in this study. Secondly, the mitigated site must exhibit a final physical shape that will not cause unacceptable downstream intensification when a UV laser beam passes through it.[12] In this study, the modulation of sites mitigated with Method A is larger than that with Method B (Fig. 6), so Method B is a better method. Thirdly, the level of residual stress in the substrate left by the protocol must be low enough that neighbour patterns (i.e. flaws and/or cracks) in the surface will not be fractured subsequently.[12] In this study, the residual stress induced by mitigation is quite small or completely eliminated after the sample has been annealed at 850 °C for 10 h in a clean furnace, which is shown in Fig. 8.

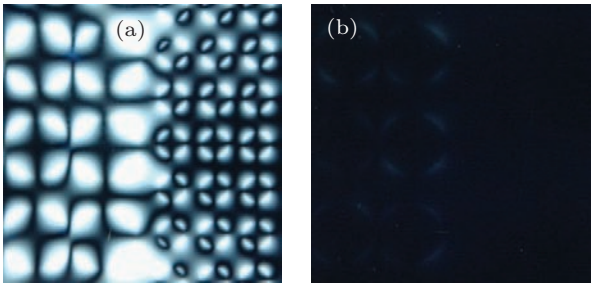


Fig. 8. (colour online) Stress images of mitigated sites before (a) and after (b) annealing the sample at 850 °C for 10 h in air.

7. Conclusion

Two mitigation methods are studied to arrest the damage growth of damage sites induced by high fluence 3ω laser irradiation. Compared with Method A (high-power, short-time, single-shot irradiation), Method B (low-power, long-time, multi-shot irradiation) is a good mitigation process. The crater conditioned with Method B has a lower depth and weaker light modulation. In addition, there is no raised rim or re-deposited debris formed around the crater edge for Method B. Theoretical calculation results of the central temperature of the CO_2 laser beam irradiated zone and the radius of crater are consistent with the experimental results. It can explain the formation of the raised rim and re-deposited debris. For Method B, a larger laser-affected zone is obtained sometimes, which can lead to a larger negative influence on the wavefront quality of optical components than the crater mitigated with Method A. Therefore, further investigation is necessary to improve the crater profile mitigated with Method B.

References

[1] Menapace J A, Davis P J, Steele W A, Wong L L, Suratwala T I and Miller P E 2005 *Proc. SPIE* **5991** 599103
[2] Davis P J, Hachkowski M R, Menapace J A, Nelson A, Steele W A and Xin K, 2006 *Proc. SPIE* **6403** 64030N
[3] Prasad R R, Bruere J R, Halpin J, Lucero P, Mills S, Bernacil M and Hackel R P 2003 *Proc. SPIE* **5373** 296
[4] Brusasco R M, Penetrante B M, Peterson J E, Maricle S M and Menapace J A 2002 *Proc. SPIE* **4679** 48
[5] Norton M A, Donohue E E, Feit M D, Hackel R P, Hollingsworth W G, Rubenchik A M and Spaeth M L 2007 *Proc. SPIE* **6403** 64030L
[6] Bouchut P, Garrec P and Pelle C 2003 *Proc. SPIE* **4932** 103
[7] Hrubesh L W, Norton M A, Molander W A, Wegner P J, Staggs M C, Demos S G, Britten J A, Summers L J, Lindsey E F and Kozlowski M R 2001 *Proc. SPIE* **4347** 553

[8] Kozlowski M, Demos S, Wu Z L, Wong J, Penetrante B and Hrubesh L 2001 *3 Damage: Growth Mitigation* Lawrence Livermore National Laboratory (LLNL), Livermore, CA 2001

[9] Hrubesh L W, Norton M A, Molander W A, Donohue E E, Maricle S M, Penetrante B M, Brusasco R M, Grundler W, Butler J A and Carr J W 2002 *Proc. SPIE* **4679** 23

[10] Mendez E, Nowak K M, Baker H J, Villarreal F J and Hall D R 2006 *Appl. Opt.* **45** 5358

[11] Palmier S, Gallais L, Commandr M, Cormont P, Courchinoux R, Lamaignere L, Rullier J L and Legros P 2009 *Appl. Sur. Sci.* **255** 5532

[12] Adams J J, Bolourchi M, Bude J D, Guss G M, Matthews M J and Nostrand M C 2010 *Proc. SPIE* **7842** 784223

[13] Xiang X, Zheng W G, Yuan X D, Dai W, Jiang Y, Li X B, Wang H J, Lü H B and Zu X T 2011 *Chin. Phys.* B **20** 044208

[14] Bass I L, Guss G M, Nostrand M J and Wegner P J 2010 *Proc. SPIE* **7842** 784220

[15] Brusasco R M, Penetrante B M, Butler J A and Hrubesh L W 2001 *Proc. SPIE* **4679** 40

[16] Brusasco R M, Penetrante B M, Butler J A, Maricle S M and Peterson J E 2002 *Proc. SPIE* **4679** 34

[17] Dai W, Xiang X, Jiang Y, Wang H J, Li X B, Yuan X D, Zheng W G, Lü H B and Zu X T 2011 *Optics and Lasers in Engineering* **49** 273

[18] Guss G, Bass I, Draggoo V, Hackel R, Payne S, Lancaster M and Mak P 2006 *Proc. SPIE* **6403** 64030M

[19] Yang S T, Matthews M J, Elhadj S, Cooke D, Guss G M, Draggoo V G and Wegner P J 2010 *Proc. SPIE* **7842** 784219

[20] McLachlan A D and Meyer F P 1987 *Appl. Opt.* **26** 1728

[21] Feit M D and Rubenchik A M 2001 *Modeling of Laser Induced Damage in NIF UV Optics* Lawrence Livermore National Labatory CA (US) 2001

[22] Feit M D and Rubenchik A M 2003 *Proc. SPIE* **4932** 91

[23] Zhao J, Sullivan J, Zayac J and Bennett T D 2004 *J. Appl. Phys.* **95** 5475

[24] Mendez E, Baker H J, Nowak K M, Villarreal F and Hall D R 2005 *Proc. SPIE* **5647** 165

[25] Li L, Xiang X, Zu X T, Wang H J, Yuan X D, Jiang X D, Zheng W G and Dai W 2011 *Chin. Phys.* B **20** 074209

[26] Runkel M, Hawley-Fedder R, Widmayer C, Williams W, Weinzapfel C and Roberts D 2005 *Proc. SPIE* **5991** 59912H

[27] Matthews M J, Bass I L, Guss G M, Widmayer C C and Ravizza F L 2007 *Proc. SPIE* **6720** 67200A